Journal of Marine Research, 66, 157–189, 2008

Journal of
MARINE RESEARCH

Volume 66, Number 2

Measuring turbulent large-eddy structures with an ADCP. 1. Vertical velocity variance

by A. E. Gargett[1,2], A. E. Tejada-Martínez[3] and C. E. Grosch[1]

ABSTRACT

Two different turbulent flows, Langmuir supercells and unstable convection, have been sampled with a VADCP, an acoustic Doppler current profiler (ADCP) with an additional vertical (V) beam. Direct measurements of the profile of vertical velocity variance provided by the vertical beam are used to calculate observational response functions for algorithms used to derive vertical velocity from the 4 beams of a standard ADCP. A theoretical response function derived for the vertical velocity estimate from a single pair of opposed slant beams illustrates the importance of large-scale quasi-coherent flow structures, as well as effects of different angles of slant beams from vertical. Different large-eddy characteristics for Langmuir supercells and unstable convection yield different theoretical response: however in both cases, the theoretical response agrees qualitatively with that derived from observations. For Langmuir supercells, there is additional agreement with numerical response functions generated by using the geometry of a VADCP to sample three-dimensional flow fields available from large eddy simulations (LES). The results from all three approaches show that there can be significant error in vertical velocity inferred from slant beam velocities. The error may be either over- or under-estimation, depending upon (usually unknown) features of the large eddies of the turbulent field, such as vertical/horizontal anisotropy, phase coherence, and orientation of horizontally anisotropic turbulent structures relative to the instrument. Given only a standard ADCP, the "best" estimate of vertical velocity variance is not the usual 4-beam estimate, but the larger of the two pair estimates.

1. Introduction

Since the early 1970s, measurements of ocean turbulence have tended to be measurements of turbulent dissipation scales, usually made from freely falling profilers (although some success-

1. Center for Coastal Physical Oceanography, Old Dominion University, Norfolk, Virginia, 23508, U.S.A.
2. Corresponding author. ***email: gargett@ccpo.odu.edu***
3. Department of Civil and Environmental Engineering, University of South Florida, Tampa, Florida, 33620, U.S.A.

ful measurements have used horizontally propelled vehicles: Gargett *et al.,* 1984; Osborn and Lueck, 1985; Thorpe *et al.,* 2003). In general, it has not been possible to measure the energy-containing scales of ocean turbulence, partly because some sensors, like airfoil probes, are band-limited by nature, but also because both freefall and self-propelled vehicles respond to motions of scales similar to their own dimensions, acting as an effective high-pass filter. However, it is often the large scales of turbulence that we most wish to know about. The structure and variability of the energy-containing turbulent scales contain direct links to the instability mechanism(s) that deliver energy to them, hence to a basic understanding of processes that generate ocean turbulence. Because of the well known three-dimensional turbulent cascades of kinetic energy and scalar variance, the dissipation scales that can be measured unfortunately contain no direct information about the processes that generated them, nor the vertical fluxes associated with them, fluxes essential for global ocean circulation and embedded ecosystems. Instead, energy-containing scales and turbulent fluxes have been inferred indirectly from measured microscale quantities using multiple assumptions, some of which are unproven or even doubtful: isotropy is unlikely for energy-containing scales, constant mixing efficiency and a single eddy diffusivity for all scalars are suspect in the case of vertical fluxes, while the flux-gradient relationship itself is unproven. It is thus highly desirable to measure the energy-containing and flux-carrying scales of ocean turbulence directly.

In shallow coastal waters, progress has been made toward this goal through deployments of bottom tripods heavily instrumented with point sensors (e.g. Christopher *et al.,* 2006). Disadvantages of this technique include inability to measure the entire water column where it exceeds the frame height (typically 1–2 m), lack of continuous vertical profiles, and mechanical fragility of the system, precluding measurements during highly energetic storm conditions. Stanton (2001) developed a sturdy bipolar acoustic system which produces continuous profiles of collinear velocity components in the near-bottom boundary layer, but the technique cannot be substantially scaled up in size to extend measurement further from the boundary (Stanton, pers. comm.), nor deployed on moorings or towed bodies. As a result there is interest in the potential of commercially available acoustic Doppler current profilers (ADCPs) for turbulence measurement.

Development of pulse-to-pulse coherent and broadband sonar systems during the late 1980s provided the accuracy needed to measure relatively small turbulent velocities in the sea. Over the past several years, both standard 4-beam ADCPs (Stacey *et al.,* 1999; Cheng *et al.,* 1999; Rippeth *et al.,* 2002; Lu and Lueck, 1999) and VADCPs, systems with an additional vertical beam (Gargett, 1994; Gargett and Wells, 2007, henceforth GW07) have been used to measure previously inaccessible characteristics of turbulence, predominantly in shallow coastal locations. Shallow deployments have many advantages as testbeds for Doppler turbulence measurements. Full water column coverage can often be obtained despite limited ranges associated with the high frequencies required for acceptable velocity resolution. Bottom deployment provides a reliably stable platform, and sufficiently shallow water allows accurate instrument orientation by divers. Finally, coastal observatories, cabled either to shore or to near-by platforms, provide sufficient power for continuous operation of ADCP systems at the necessary sample rates.

Provided significant issues of platform stability, automatic level adjustment, and power supply can be met, it is hoped to move such techniques to other platforms (stiff moorings, ultra-stable towed bodies).

For both present shallow water deployments as well as future deep water measurements, the spatial arrangement of acoustic beams is a fundamental determinant of the ability to measure turbulence. Ideally, one would profile all three components of the instantaneous velocity vector along a vertical line. Instead, a standard Janus-configuration ADCP measures radial velocities along pairs of opposing beams in two orthogonal planes, aligned respectively along x and y (instrument-based) axes. Each beam in a pair makes an angle θ with the vertical z-axis[4], defined with zero at the face of the transducer array. The centers of paired beams are separated by a distance $2\Delta(z) = 2z \tan\theta$ that increases with z. Under an assumption that the velocity field is uniform across the full beam spread (first-order homogeneity), estimates of horizontal velocity components are made from pairs of slant beams, while the standard estimate for vertical velocity uses all four beams. An assumption of uniformity over beam spread is reasonable for large-scale time-mean velocity fields, but less comfortable for turbulence scales, which may be comparable to or smaller than the size of the 4-beam footprint at a particular height. It is thus of considerable interest to better understand the nature of the spatial response of an ADCP for all six turbulent stresses (three normal stresses (variances), and three shear stresses) as functions of height and underlying turbulent structure.

Of the velocity component variances that make up the turbulent kinetic energy per unit mass E, vertical velocity variance is particularly crucial to the dynamics of turbulence in a stratified fluid, where buoyancy forces remove energy preferentially from the vertical component of E. This paper reviews possible estimates of turbulent vertical velocity variance that can be made from the slant beam velocities of an ADCP (Section 2) and uses various methods to quantify the degree to which the typical Janus configuration affects these estimates. Subsequent papers will address horizontal variances and shear stresses.

In Section 3, we examine observational data from a 1.2 MHz broadband VADCP deployed in 15 m of water at the LEO15 cabled observatory off the coast of New Jersey. The vertical beam was aligned to within 0.2° of vertical in both pitch and roll during the measurements reported here, hence provides an unequivocal measure of vertical velocity with which to compare slant-beam estimates. Two different turbulent flows generate measurable vertical velocities at this site. Langmuir supercells, LSC, (Gargett *et al.,* 2004; GW07) are generated during episodes of strong wind/wave forcing of a non-stratified water column, while "pure" unstable convection requires weak winds and minimal surface waves in addition to unstable surface buoyancy forcing. Section 3 describes distinctive features of these two flows, then derives observational response functions as ratios of slant-beam vertical velocity variance to the

4. Depending on the strength and frequency/wavenumber content of the flow field within which a turbulent field is embedded, instrument misalignment leads to irrevocable contamination of the turbulent field measurement. In this paper, it is assumed that the instrument has been accurately aligned to vertical, so fields calculated from combinations of slant beam velocities do not contain errors due to alignment, and the vertical fifth beam of a VADCP directly measures vertical velocity.

true variance of the vertical beam measurement. To aid understanding of factors influencing the response, Section 4 explores a theoretical response function derived from simplified velocity structures that include significant aspects of turbulent large eddies. In Section 5, we derive response functions in a third way, by sampling numerical flow fields produced by large-eddy simulations (LES) of LSC (Tejada-Martínez and Grosch, 2007, henceforth TMG07) with the geometry of an ADCP. Section 6 compares the LES and observational response functions for the LSC case, while Section 7 assesses predictive ability of the theoretical response for both LSC and convection. Section 8 summarizes important characteristics of the response function for slant-beam estimation of turbulent vertical velocity variance, as revealed by the combination of the three independent methods used to estimate response. We emphasize features of the turbulent field that most affect response and suggest the best estimate to use in absence of *a priori* information about some of these important features.

2. Algorithms for determining vertical velocity from ADCP measurements

Consider the three-dimensional velocity field $\underline{u}(x, y, z) = (u, v, w)$ in an instrument-based coordinate system with origin at the transducer face(s), z positive upward, x positive in the direction from beam 2 toward beam 1, and y positive from beam 4 toward beam 3 (directed 90° to the right of beam 2; see GW07, Fig. 1(a)). In this system, slant beam velocities (defined as positive if directed toward the transducer) at height z are given by

$$B_1 = -u(+\Delta(z), 0, z)\sin\theta - w(+\Delta(z), 0, z)\cos\theta \tag{1}$$

$$B_2 = u(-\Delta(z), 0, z)\sin\theta - w(-\Delta(z), 0, z)\cos\theta \tag{2}$$

$$B_3 = -v(0, +\Delta(z), z)\sin\theta - w(0, +\Delta(z), z)\cos\theta \tag{3}$$

$$B_4 = v(0, -\Delta(z), z)\sin\theta - w(0, -\Delta(z), z)\cos\theta \tag{4}$$

and vertical velocity is directly measured by the vertical beam,

$$w(0, 0, z) = -B_5. \tag{5}$$

In statistically stationary turbulence, velocity $\underline{u} = \underline{U} + \underline{u}'$ is assumed to consist of two parts, a mean field $\underline{U}(z) = (U(z), V(z), 0)$ that is a function only of z, and a three-dimensional fluctuating field $\underline{u}'$ with zero mean $\langle \underline{u}' \rangle = 0$ and turbulent kinetic energy per unit mass $E = \frac{1}{2}\langle u'u' + v'v' + w'w' \rangle$, where angle brackets denote a suitable averaging process[5]. In this case, the beam velocities $B_q = \langle B_q \rangle + B_{qf}$, $q = 1, \ldots, 4$ are

5. The fluctuating velocity structures that can be observed at LEO15 must have periods longer than surface wave periods (from which they are separated by low pass filtering), and shorter than the dominant semi-diurnal tidal period. Because stable statistics typically require averaging over periods greater than an hour (see GW07) and tidal velocities can vary over this period, a linear least squares fit, computed separately at each bin, is first removed from the beam velocity time series. The averaging operator $\langle\,\rangle$ denotes a subsequent time average over a period of one record (~ 2 h: individual records are referenced as sss.nnn, where nnn is the number of the record within session sss).

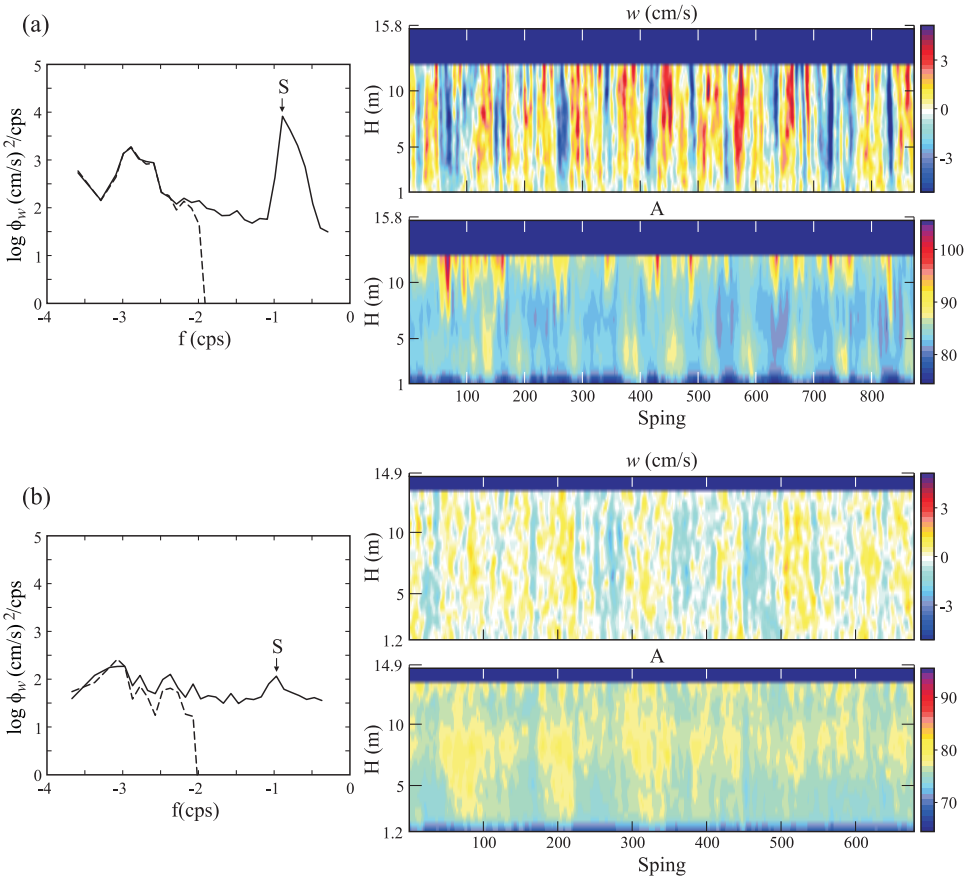

Figure 1. Left: Frequency spectra of w', the fluctuation vertical velocity measured by a vertical sonar beam from a mid-depth bin of the record to the right: (a) Langmuir supercells, record 043.024, ~ 2.3 h (b) unstable convection, record 161.008, ~ 1.8 h. The complete spectrum (solid line) contains a high frequency surface wave peak (S) of varying amplitude and period which is removed by low-pass filtering (filtered spectrum, dashed line), leaving the w fields seen in the right panels. Right: color maps of (top) w' and (bottom) vertical beam backscatter amplitude A (corrected for geometric spreading and absorption, but uncalibrated). The top of the panels coincides with mean surface depth, respectively 15.8 m and 14.9 m. Missing data below the mean surface result from wave-induced variation of the instantaneous surface: larger surface waves in (a) lead to the greater loss of filtered data near the surface. The scale for w' ($\pm$4 cm/s) is the same for both flows: the scale for A varies with the type and amount of scattering elements present.

also made up of two parts, a mean $\langle B_q(z)\rangle$ and a fluctuating part $B_{qf}(x, y, z)$ with zero mean $\langle B_{qf}\rangle = 0$ and variance $\langle B_{qf}^2\rangle$. With these assumptions, Eqs. (1)–(5) can be written for both mean and fluctuating components individually. Assuming first-order homogeneity, i.e. that velocity structures have horizontal scale very much larger than the distance

between beams, so that $u(-\Delta, 0, z) = u(\Delta, 0, z)$ and $v(0, +\Delta, z) = v(0, -\Delta, z)$, Eqs. (1)–(4) written for the fluctuating components can be used to make a first-order full-spread (subscript F) estimate of vertical velocity

$$w'_F = -\frac{\sum_{i=1}^{4} B_{if}}{4 \cos \theta} \tag{6}$$

as a function of z[6]. This estimate, the usual one reported from 4-beam ADCP data, is the average of independent estimates made from beam pairs, i.e.

$$w'_x = -(B_{1f} + B_{2f})/2 \cos \theta \tag{7}$$

and

$$w'_y = -(B_{3f} + B_{4f})/2 \cos \theta. \tag{8}$$

To assess the quality of w' estimated with ADCPs, three estimates of vertical velocity variance, computed as the squares of Eqs. (6), (7) and (8), are compared with the true value given by the square of the fluctuating form of Eq. (5), i.e.

$$\langle w'^2 \rangle = \langle B_{5f}^2 \rangle. \tag{9}$$

3. Observational determination of response functions

The right-hand panels of Figure 1 illustrate characteristic features of w' and backscatter amplitude (A) fields for the two turbulent flows considered here. During an episode of Langmuir supercells (LSC, Fig. 1(a)), the backscatter field exhibits distinctive clouds of high backscatter originating both from the surface, where they are attributed to air microbubbles from breaking waves and correlated with downward vertical velocity, and from the bottom, where they are assumed to be caused by resuspended sediment and associated with upward vertical velocity. As discussed by Gargett *et al.* (2004) and simplified in the cartoon of Figure 2, there are strong phase relationships among the velocity components of the large eddies of LSC when viewed in horizontal coordinates aligned with (x_1) and across (x_2) the wind. The observed three-dimensional velocity field (with horizontal velocities derived assuming first-order homogeneity) is consistent with the presence of pairs of counter-rotating cells, elongated in the downwind direction, with surface convergence into and bottom divergence out of downwellings. A downwind jet is located over downwellings, with diminished downwind flow over upwellings.

Vertical velocities associated with convective instability, typified by the case seen in

6. Surface returns in vertical sidelobes of the slant beams have the potential to contaminate slant beam velocities, hence any variables calculated with them, for $z > z_s = H\cos\theta$, where H = surface height above the transducer.

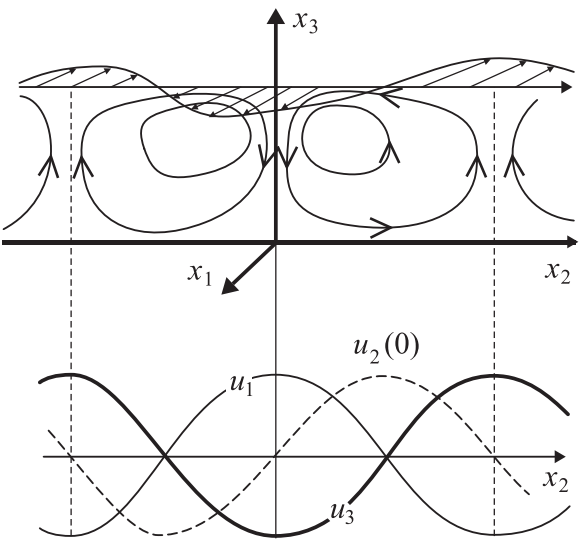

Figure 2. Upper: Cartoon of the structure of Langmuir supercells, shown in wind coordinates $\{x_1, x_2, x_3\}$, where x_3 is positive upward, x_1 is positive in the downwind direction, and x_2 completes a right-handed coordinate system. Lower: Idealized $\{u_1, u_2, u_3\}$ velocity components near the bottom of the water column. At the top of the water column, the phase of u_2 is reversed, i.e., $u_2(H) = -u_2(0)$.

Figure 1(b), are weaker and accompanied by mid-depth backscatter maxima associated predominantly with upward vertical velocity[7], a very different pattern from that of LSC. In the convective case, horizontal velocity variances are of roughly equal magnitude throughout the measured water column, independent of the horizontal coordinate system (instrument, geographic, wind or current) used, hence are horizontally isotropic.

For both flows, low frequency peaks in the spectral plots of Figure 1 occur at an apparent frequency f set by the time interval T taken for tidal and/or wind-driven mean flow of magnitude $|\underline{U}| = (U_x^2 + U_y^2)^{1/2}$ to advect a turbulent large-eddy structure with characteristic spatial scale L past the fixed location of the VADCP. If turbulent large-eddies are horizontally isotropic, measurements of f and $|\underline{U}|$ provide an accurate estimate of the dominant spatial scale. In the convective case of Figure 1(b), where horizontal isotropy is strongly indicated by equality of horizontal velocity variances, independent of coordinate orientation, $L \sim |\underline{U}|/f \sim (0.08 \text{ m/s})/(1 \times 10^{-3} \text{ cps}) \sim 80$ m. However when large-eddy structures are strongly anisotropic, orientation of the structures relative to the mean velocity must be taken into account when deriving spatial scale from apparent frequency. As an example, consider the idealized Langmuir circulation, invariant in the downwind

7. The origin of these maxima are unknown, but they may be due to scattering from density microstructure (Thorpe and Brubaker, 1983; Goodman, 1990) associated with entrainment at the edges of cold downwelling plumes.

direction, of Figure 2. A fixed sensor will not register fluctuations due to wind-aligned large-eddy structures unless there is non-zero crosswind mean flow U_y. At LEO15, tidal flow produces crosswind advection that modulates the apparent frequency of LSC in the observations (GW07). In the case shown (Fig. 1(a)), the relevant (crosswind) wavelength of the structures is given by $L_y = U_y/f \sim (0.13 \text{ m/s})/(1.5 \times 10^{-3} \text{ cps}) \sim 80$ m.[8] Thus for the records shown in Figure 1, the horizontal scales of the (isotropic) convective structures and the crosswind structure of the (anisotropic) LSC are similar in magnitude.

For the two flow regimes described above, the left-hand panels of Figure 3 compare the profile of the variance of vertical velocity determined directly from the vertical beam with those of the three estimates w'_F, $\langle w'^2_y \rangle$ and $\langle w'^2_x \rangle$: all variances have been corrected for noise bias (Appendix A). To avoid impossible complexity in the figure, statistical error bars are not shown, but are illustrated for representative records in Appendix A. Although details vary, the major features of these individual records are common to all records that can be clearly classified into the stated categories.[9] For all examined cases of LSC, the three slant beam estimates of vertical velocity variance are generally less than $\langle w'^2 \rangle$ throughout the accessible water column. The minimum estimate is normally the "isotropic" estimate $\langle w'^2_F \rangle$. In LSC records, the two slant beam pair estimates may differ significantly[10]: in the case shown in Figure 3(a), they are roughly equal below $x_3/H \sim 0.2$, but diverge higher in the water column. Over the range $x_3/H \sim (0.4\text{–}0.75)$, $\langle w'^2_y \rangle < \langle w'^2_x \rangle$, i.e. the estimate made from the {4,3} beam pair significantly exceeds that made from the {2,1} beam pair. This ordering is not consistent however: in other LSC records, variance ordering is reversed and in still others (e.g. Fig. 3(b)), the two variances are equal within error bounds. In all convective cases, the 4-beam estimate is again the smallest, but the two pair estimates consistently equal each other and $\langle w'^2 \rangle$ within error bounds throughout the water column.

An observationally-based response function can be defined as the ratio of a slant beam variance estimate to vertical beam variance, e.g. $Rw_x \equiv \langle w'^2_x \rangle / \langle w'^2 \rangle$ for the estimate from the beam pair in the x-z plane (Eq. 7): response functions for the three slant beam estimates are shown in the right-hand panels of Figure 3. All three response functions are relatively uniform with range for both types of flow (the record of 3(b) exhibits the most extreme variation with range of all records examined), an unforeseen and quite surprising result. For a velocity structure in which horizontal scale is approximately uniform in the vertical and not very much larger than the maximum beam spread, it has been generally expected that velocities calculated from slant beams become increasingly under-estimated as slant beam separation increases. This expectation stems from Theriault (1986), who assumed

8. Note that this scale is considerably smaller than the value of $L \sim |\underline{U}|/f \sim 200$ m that would result from assuming isotropic structures.

9. Wells and Gargett (in preparation) derive a scheme that identifies records dominated by LSC and unstable convection based on external forcing parameters.

10. Average values that differ by more than their associated (one standard deviation) error bounds (see Appendix A) are considered to be significantly different.

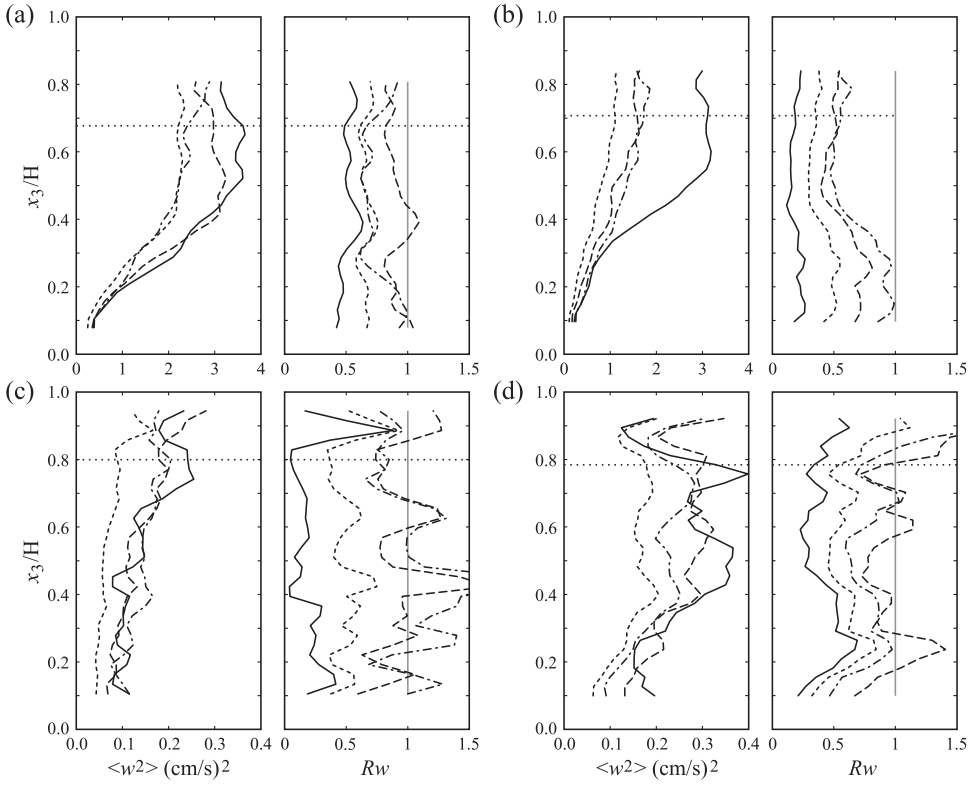

Figure 3. Left panels of each set: Variances of vertical velocity as determined from: a vertical acoustic beam ($\langle w'^2 \rangle$, solid line), the {2,1} slant beam pair ($\langle w_x'^2 \rangle$, dot-dash line), the orthogonal {4,3} slant beam pair ($\langle w_y'^2 \rangle$, long dash line), and all four slant beams ($\langle w_F'^2 \rangle$, short dash line). Variances are averages over the time extent of a single record ($\sim$ 2 h) and are corrected for noise bias (Appendix A). Right panels: Response functions for individual slant-beam pair estimates $Rw_x = \langle w_x'^2 \rangle / \langle w'^2 \rangle$ (dot-dash line), $Rw_y = \langle w_y'^2 \rangle / \langle w'^2 \rangle$ (long dash line), and the 4-beam estimate $Rw_F = \langle w_F'^2 \rangle / \langle w'^2 \rangle$ (short dash line). Solid line: normalized covariance $\langle w_x' w_y' \rangle / \langle w'^2 \rangle$ between the two slant beam pair estimates. The horizontal line in each panel marks z_s, the height above which sidelobe reflections can potentially contaminate velocities computed from the slant beams. Langmuir supercells: (a) Record 043.024 (b) Record 154.011. Unstable convection: (c) Record 161.007 (d) Record 161.008.

zero vertical velocity and derived a response function for horizontal velocity that falls steeply with increasing range. However using Theriault's methods but modifying the form of assumed velocity fields to better represent turbulence, Gargett (1994, see Appendix 1) derived a horizontal velocity response function that could be either less than or greater than unity, depending on both an anisotropy ratio, defined as the ratio of the vertical and horizontal velocity component magnitudes, and the possibility of consistent phase relationships between these components. In the following section, we explore characteristics of a

similar theoretical response function derived for the vertical velocity estimated from a single beam pair.

First, however, we address a general question arising from Figure 3, namely why $\langle w'^2_F \rangle$ is typically smaller than both slant beam pair variances. Since w_F is the average of the two pair estimates, the four-beam variance estimate

$$\langle w'^2_F \rangle = \tfrac{1}{4} \langle (w'_x + w'_y)^2 \rangle = \tfrac{1}{4} (\langle w'^2_x \rangle + \langle w'^2_y \rangle + 2\langle w'_x w'_y \rangle),$$

will equal the true variance $\langle w'^2 \rangle$ only if $\langle w'^2_x \rangle = \langle w'^2_y \rangle = \langle w'_x w'_y \rangle = \langle w'^2 \rangle$, ie if both of the pair variances *and* the covariance between pair estimates all individually equal the true variance. However the observations indicate that the pair covariance (shown normalized by the true variance as solid line profiles in the right panels of Fig. 3) is always less than the pair variances, reducing the four-beam estimate relative to either pair estimate.

4. Theoretical response function for vertical velocity estimated from a slant beam pair

A theoretical response function $Tw(k, z)$ for the vertical velocity estimate w'_x made from a single beam pair depends at minimum on the dominant horizontal wavenumber k of the velocity field and height z. Following Gargett (1994), consider simple forms $u' = u_o \exp i(kx)$ and $w' = w_o \exp i(kx + \phi_o)$ for the velocity components that appear in the beam velocities used in Eq. (7) for w'_x[11]. These simplified velocity fields are intended not as an accurate descriptor of turbulent velocity fields, but as a tool to explore what features of turbulent fields have significant effects on response. The forms chosen allow for possible phase differences between u' and w', as well as anisotropy in the sense of differences in amplitude between horizontal and vertical velocity components: both are essential characteristics of large eddies of turbulent flows.

The resulting vertical velocity response function

$$Tw(k, z) \equiv \frac{w'_x (w'_x)^*}{w_o^2} = \cos^2 k\Delta + \frac{1}{r^2} \sin^2 k\Delta + \frac{1}{r} \sin 2k\Delta \sin \phi_o, \qquad (10)$$

where (*) denotes complex conjugation, depends not only on k and z (through the half-beam separation $\Delta(z)$), but also on phase angle ϕ_o by which the vertical velocity component leads or lags the horizontal velocity component and on the magnitude of w_o/u_o, which we term the anisotropy ratio, through the parameter $r \equiv w_o \cot \theta / u_o$[12].

As seen in Figure 4, Tw is strongly influenced by both r (or equivalently for fixed θ, by

11. Variation in the y-dimension, normal to the plane of the {2,1} beam pair, does not affect velocities based on this pair, hence $Tw(k, z)$ is independent of v'.

12. This form of r is used for compatibility with previous derivations of response functions for the horizontal velocity component (Theriault, 1986; Gargett, 1994), which use this form to allow determination of the u-response in the limit of $w \to 0$ ($r \to 0$). The limit $r \to 0$ is not allowed when the w-response function is being considered.

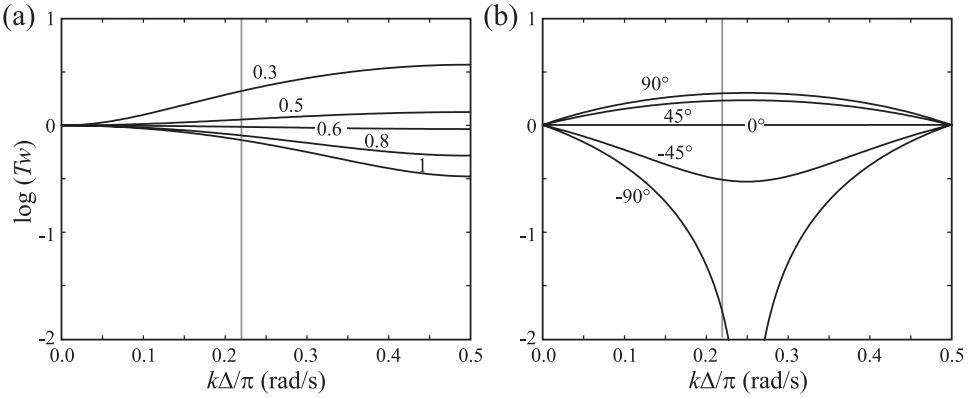

Figure 4. Logarithm of a theoretical response function Tw for vertical velocity variance calculated from a single beam pair, as a function of normalized wavenumber $k\Delta/\pi$, where $k = 2\pi/L$ is the horizontal wavenumber associated with horizontal length scale L and $\Delta(z) = z \tan\theta$ is the half-spread for slant beams at an angle of $\theta = 30°$ from vertical. The solid vertical line marks the value of $k\Delta_M/\pi$ for the wavenumber $k = 2\pi/80$ m that is associated with observed convective structures and LSC crosswind structure and $\Delta = \Delta_M = (15\text{ m})\tan 30°$, the maximum LEO15 half-spread. Response (a) as a function of noted values of anisotropy ratio w_o/u_o for fixed phase ($\phi_o = 0°$ *or* $180°$) between vertical and horizontal velocity components in the plane of the beam pair; (b) as a function of noted values of phase ϕ_o for the fixed anisotropy ratio $w_o/u_o = 0.577$ that yields unity response for zero phase.

w_o/u_o) and ϕ_o.[13] Figure 4(a) shows Tw as a function of normalized wavenumber $k\Delta/\pi$ (chosen for ease of comparison with the results of Theriault (1986) and Gargett (1994)) for fixed $\phi_o = 0°$ (or 180°) and a range of w_o/u_o. Unit response occurs for $w_o/u_o \simeq 0.577$ (corresponding to $r = 1$ in Eq. (10)): for smaller/larger values of w_o/u_o, the response is greater/less than unity. For the wavenumber $k = 2\pi/80$ m that characterizes both convection and LSC (crosswind) scales at LEO15, a vertical line indicates the maximum value of $k\Delta_M = kH\tan\theta$, which occurs at the water column height $H \sim 15$ m. For a structure of fixed horizontal wavenumber over depth, Tw_x is unity at $k\Delta = 0$ ($z = 0$) independent of k, then either decreases or increases as $\Delta \rightarrow \Delta_M$, depending on whether w_o/u_o is (and remains) above or below $w_o/u_o = 0.577$. This relatively simple behavior can be dramatically modified by the presence of non-random phase relationships between the two velocity components, as illustrated in Figure 4(b) using the fixed value of $w_o/u_o = 0.577$ that for $\phi_o = 0°$ gives unity response. Negative phase between w' and u' (defined as w' lags u' in the sense that u'_3 lags the bottom variation of u'_2 in Figure 2(b)) results in under-estimation of vertical velocity, while positive phase causes over-estimation. The magnitude of the phase effect depends on the value of w_o/u_o. As w_o/u_o falls below 0.577, the $-90°$ curve falls more rapidly and the $+90°$ curve rises more rapidly; changes are

13. Note that both variables may be expected to vary with height above the bottom in a real flow.

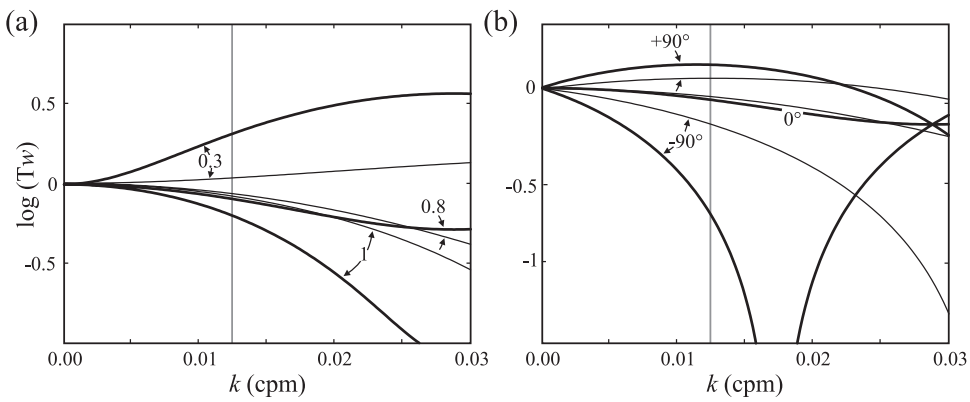

Figure 5. Comparison of theoretical vertical velocity response functions for pairs of slant beams with angles from vertical of $\theta = 30°$ (heavy lines) and $\theta = 20°$ (light lines), calculated for $\Delta = \Delta_M =$ (15 m) tan 30°, the maximum LEO15 half-spread. The vertical line denotes the dimensional wavenumber associated with the value of $k = 2\pi/80$ m estimated for observed convective structures and LSC crosswind structure. (a) Variation with w_o/u_o (0.3, 0.8, 1) for fixed $\phi_o =$ 0°(180°). (b) Variation with ϕ_o (−90°, 0°, +90°) for the value $w_o/u_o = 0.8$. at which the zero phase response of the geometries is approximately equal.

opposite as w_o/u_o rises above 0.577. A response profile is the net result of z-variation of both w_o/u_o and ϕ_o; however for observed degree of variations in both parameters, effects of changes in w_o/u_o are secondary in the presence of significant phase variation.

The theoretical function enables comparison between the responses of systems with different slant beam angles from vertical: older instruments, such as that used at LEO15, have $\theta = 30°$ but $\theta = 20°$ has since become a commercial standard. Variance response function comparisons in Figure 5, calculated for the worst case of maximum beam spread Δ_M and presented as functions of dimensional wavenumber k, demonstrate superior performance of the 20° angle for measurement of vertical velocity. This behavior is expected, since the slant beam velocity *becomes* the vertical velocity in the limit as $\theta \to 0$. However one cannot conclude that the smaller the slant beam angle from vertical, the better the overall turbulence measuring ability, since improved vertical variance measurement comes at the price of degradation of the measurement of horizontal velocity variances, the subject of a future manuscript.

5. Numerical response functions for LSC turbulence, as derived from LES

The three-dimensional stationary flow fields produced by LES of Langmuir-vortex-forced turbulence in shallow water (TMG07) offer an independent method of exploring slant beam response functions in the general case where beam planes make an angle ψ with the long axis of the horizontally anisotropic large-eddy structures characteristic of LSC. Simulations are available for two values (0.4 and 0.7) of turbulent Langmuir number $La_t \equiv$

$(u_\tau/u_s)^{1/2}$, where $u_\tau = (\tau_s/\rho_o)^{1/2}$ is surface friction velocity (τ_s is surface wind stress magnitude and ρ_o water density) and u_s is surface Stokes drift velocity (McWilliams *et al.,* 1997, TMG07). Forcing values of u_τ and u_s are representative of conditions producing LSC: stress forcing was held constant, so a smaller La_t corresponds to stronger Langmuir-vortex-forcing. For arbitrary ψ, the five slant-beam variances are first constructed from LES variances and covariances (averaged over time and both horizontal dimensions) at the locations of the beams in physical space: for details, see Appendix B. The computed beam variances are then used to form the slant-beam estimates of Eqs. (6)–(8) which provide numerically derived response functions (Lw) when normalized by true LES vertical velocity variance.

Our motivations for using the LES in this way are fourfold. First, it offers a direct means of determining the effect of non-zero ψ in cases with horizontal structural anisotropy of the turbulent large-eddies. Second, the LES-derived response functions may be compared with theoretical predictions without uncertainties associated with the observational responses (notably the observational values of ψ). Third, the LES can be re-sampled with different slant beam geometry, allowing a comparison with theoretical predictions of the effect of slant beam angle θ that is not available from the ($\theta = 30°$) observations. Finally, and most importantly, if the LES-derived response functions for vertical velocity variances compare well with those derived from theory and observations, we will have confidence in subsequent use of LES-derived responses as "truth" for other turbulent quantities, such as horizontal velocity variance and shear stresses, for which there is no available observational "truth" like that provided for vertical velocity by the vertical beam measurement.

For the two available values of La_t (0.4 and 0.7), Figure 6 presents normalized vertical velocity variance profiles and associated response functions for $\psi = 0°$, the case of instrument axes aligned along and across the downwind direction. The downwind pair estimate (green line) is closest to the true variance, while the crosswind pair (red line) is an under-estimate by 40–50% at depth, changing to an over-estimate as the surface is approached. Fortunately, the LES responses exhibit only weak dependence on La_t. With decrease in La_t (stronger Langmuir vortex forcing), the heights at which downwind and crosswind variances change from under-estimation to over-estimation both move closer to the surface and under-estimation by the downwind pair increases. The fully three-dimensional LES velocity fields make it possible to determine that increased under-response of the downwind pair at smaller La_t results from weaker downwind coherence of u'_1 at large Δx_1, caused by increased meandering of the Langmuir streaks relative to the downwind direction. Since increased meandering produces more isotropic large-eddy structure, it is reasonable that responses of the two beam pairs become somewhat more similar in this case.

For non-zero ψ, responses can differ substantially from the wind-aligned case. Figure 7 presents results for the maximum meaningful angle of $\psi = 45°$ (for larger ψ, the long axis of the large eddies merely becomes better aligned with the orthogonal (y) instrument axis).

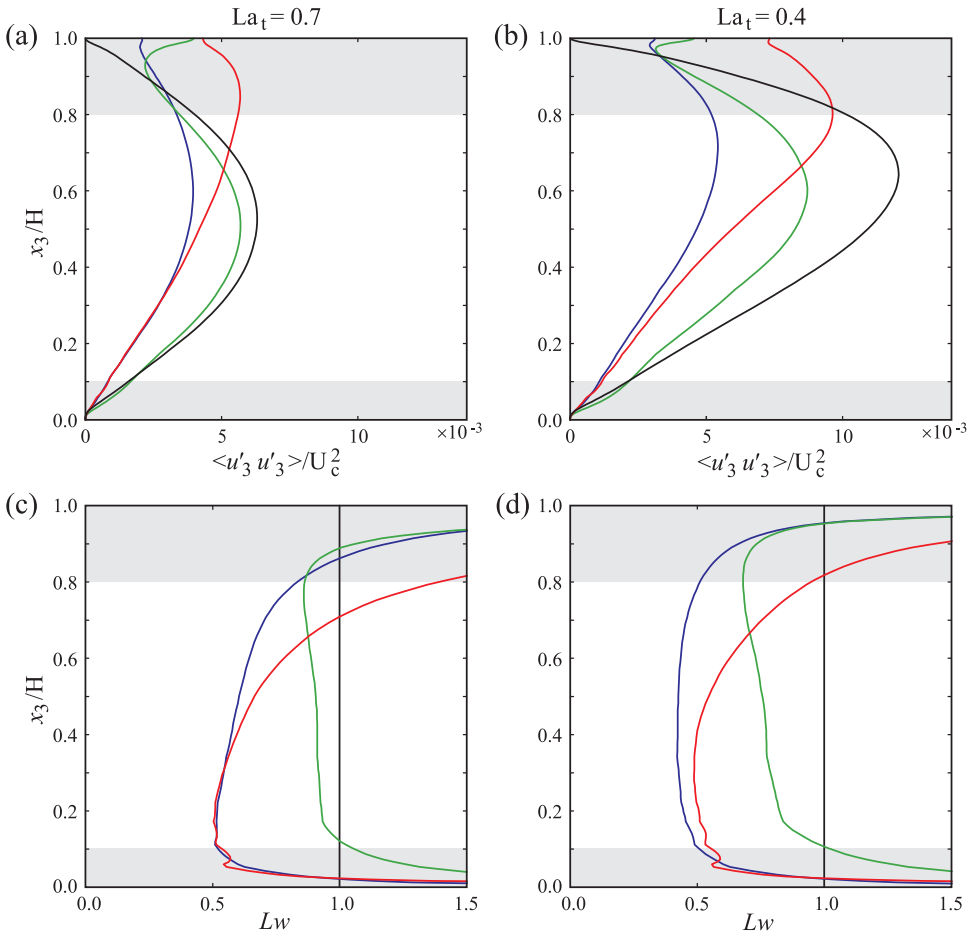

Figure 6. Variances of vertical velocity calculated by sampling LES simulations of LSC with the geometry of an ADCP: for the case $\psi = 0°$, where ψ is the angle between the instrument x-axis and the downwind (x_1) axis. Angle brackets denote averages over time and horizontal dimensions: variances $\langle u'_3 u'_3 \rangle$ in wind coordinates are normalized by the square of mean downwind velocity U_c at mid-depth. Top panels: true variance $\langle u'^2_3 \rangle = \langle w'^2 \rangle$ (black line) and estimates from the downwind slant beam pair $\langle u'^2_3 \rangle = \langle w'^2_x \rangle$ (green line), the crosswind slant beam pair $\langle u'^2_3 \rangle = \langle w'^2_y \rangle$ (red line), and all four slant beams $\langle u'^2_3 \rangle = \langle w'^2_F \rangle$ (blue line), for turbulent Langmuir number $La_t = 0.7$ (left) and $La_t = 0.4$ (right). Bottom panels: corresponding response functions, $Lw_x = \langle w'^2_x \rangle / \langle w'^2 \rangle$ (green line), $Lw_y = \langle w'^2_y \rangle / \langle w'^2 \rangle$ (red line), $Lw_F = \langle w'^2_F \rangle / \langle w'^2 \rangle$ (blue line). Grey-shaded parts of the water column are those unavailable to the LEO15 observations.

As expected when both instrument axes receive approximately equal contributions from both downwind and crosswind velocity components, the two pair estimates are nearly identical: actual values are intermediate between those of the downwind and crosswind components seen in Figure 6. Thus if large-eddy structures are horizontally anisotropic, it

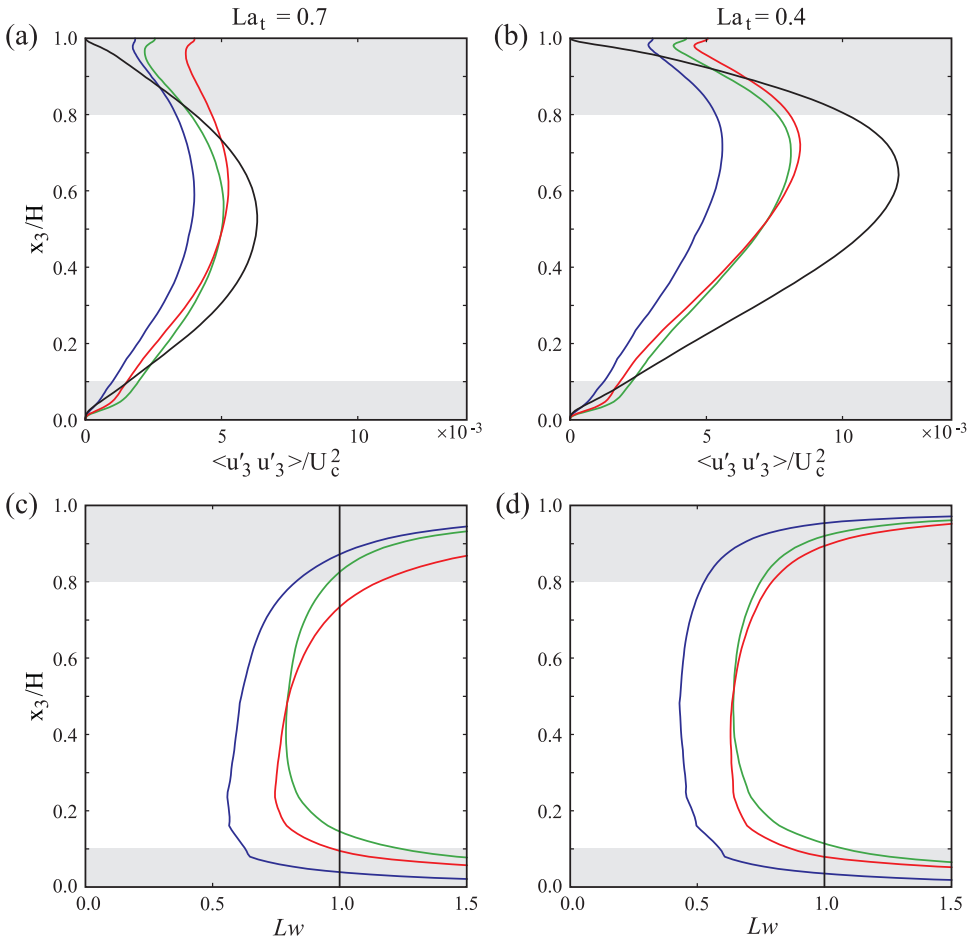

Figure 7. As in Figure 6, except $\psi = 45°$, i.e. the instrument axes make angles of 45° with wind-oriented horizontal coordinates.

is necessary to know the approximate orientation of the structures relative to instrument axes in order to estimate response using the theoretical form.

Finally, Figure 8 compares LES-derived responses for instrument slant beam angles of $\theta = 30°$ and 20°, $\psi = 0°$. The smaller beam angle improves the crosswind response, in agreement with the theoretical prediction (Fig. 5(b)). The downwind response with $\theta = 20°$ is marginally worse than that with 30°, again in agreement with the theoretical response (Fig. 5(a)) which predicts decreased under-estimation with 30° for the values of $w_o/u_o \sim 0.5$–0.7 that characterize mid-depths (not shown). In both cases, the downwind pair provides the best estimate of the true vertical velocity variance. In this situation (instrument aligned with anisotropic large-eddy structure), the difference between the

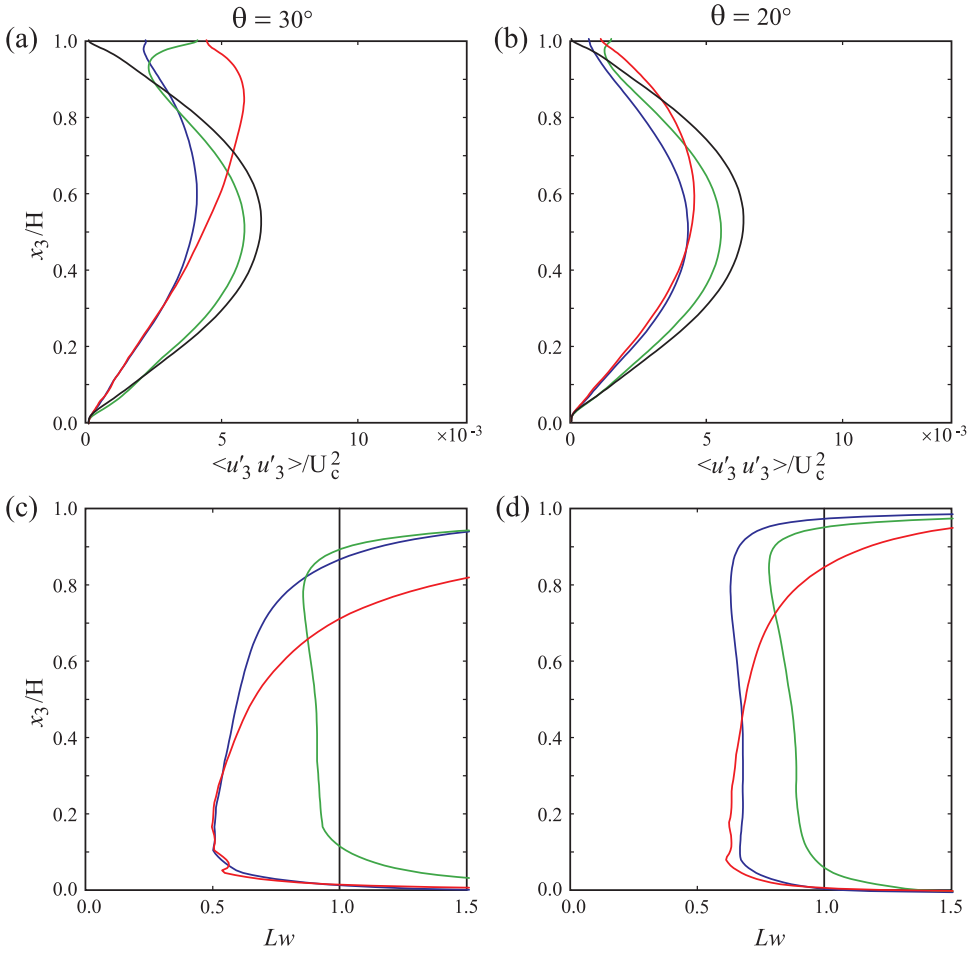

Figure 8. Comparison of profiles of vertical velocity variance (top panels) and associated response functions (bottom panels) for different angles of the slant beams from vertical, for the case La_t = 0.7, ψ = 0°. (a) and (c): θ = 30°, the angle of the LEO15 VADCP. (b) and (d): θ = 20°, the standard in most present commercial units. Notation and various curves are as described in the caption to Figure 6.

downwind pair estimate and either the crosswind pair or 4-beam estimate greatly exceeds the effect on the downwind ("best") estimate of reducing slant beam angle from 30° to 20°.

6. Comparison of LES and observational response functions for LSC

In all the LES cases, the minimum response is that of the 4-beam estimate, in agreement with observations. To assess how well other features of the LES results agree with observed LSC response functions shown in Figure 3(a) and (b), it is necessary to estimate

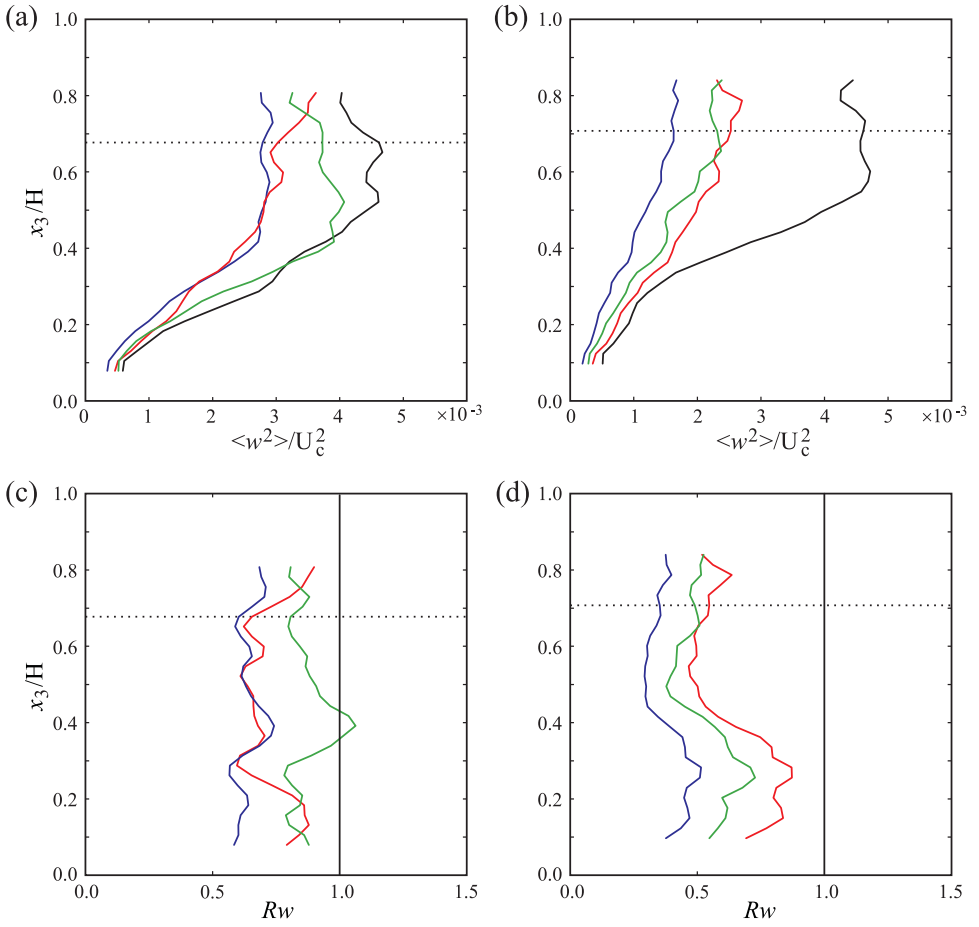

Figure 9. Vertical velocity variance profiles (upper panels), normalized by the square of observed mean downwind velocity U_c at mid-depth for direct comparison with the LES profiles in Figures 6 and 7, and associated response functions (lower panels) for the LSC records 043.024 (left) and 154.011 (right) of Figure 3. The horizontal dashed line marks z_s.

values of ψ and La_t for the two records. If it is assumed that the long axis of the LSC structures are aligned downwind (and that the wind direction measured at a nearby shore tower is accurate, see GW07), then ψ values are obtained from the known instrument axes alignment ($x = \{2,1\}$ axis toward 175°) and the downwind direction δ. For record (a) 043.024, $\delta_a = 246°$, hence $\psi_a = 71°$, while for record (b) 154.011, $\delta_b = 222°$, hence $\psi_b = 47°$. GW07 suggest that the structures may actually be aligned slightly (a few to several) degrees to the right of the wind; if so, ψ_a will be slightly closer to 90°, ψ_b slightly further from 45°.

Determination of an appropriate value of La_t is complicated by the fact that surface waves are characterized by a spectrum, rather than the single frequency used by GW07 to

compute values of $La_t \sim 0.5$ for 043.024 and $La_t \sim 0.7$ for 154.011. However, the LES results of Figures 6 and 7 show that the vertical velocity variance profile varies with La_t, exhibiting a nearly symmetrical profile about a mid-depth maximum for $La_t = 0.7$ but an asymmetrical profile with maximum nearer the surface for $La_t = 0.4$. Observed profiles of "true" LSC vertical velocity variance $\langle w'^2 \rangle$ (shown in Fig. 9 normalized by the square of observed mean velocity U_c at mid-depth to allow direct comparison with the LES profiles in Figs. 6 and 7) have maximum values comparable to the $La_t = 0.7$ case, but are distinctly asymmetric about mid-depth. The appropriate value of La_t for both records thus appears to lie somewhere between 0.4 and 0.7.

For record 043.024, we assume $\psi_a \sim 90°$ (since $\psi_a = 71°$ may be somewhat underestimated, see above), which is equivalent to $\psi = 0°$ with the $y = \{4,3\}$ axis rather than the $x = \{2,1\}$ axis aligned with the wind direction. We thus compare observed variances with the LES results for $\psi = 0°$, interpreting observed $\langle w_y'^2 \rangle$ as downwind and $\langle w_x'^2 \rangle$ as crosswind. The observed variance profiles and associated response functions have the following features in common with the LES results of Figure 6. (1) The downwind estimate is the most accurate within the accessible part of the water column. (2) Crosswind and 4-beam estimates tend to be comparable in magnitude and smaller than the downwind estimate. (3) The downwind pair estimate shows a tendency to decrease and fall below the (still increasing) crosswind pair above $x_3/H < 0.75$, a crossover point consistent with that seen in the two LES (although the actual crossover point is above z_s, the height of potential sidelobe interference, tendency for the two estimates to converge starts below this level). For record 154.011, we compare observed variances with the LES results for $\psi = 45° \sim \psi_b$. The two observational pair estimates show a comparable degree of underestimation, in agreement with the LES results seen in Figure 7. Neither LSC case shows response crossover from under- to over-estimation within the accessible part of the water column, a result which would agree with the LES result if the La_t values were closer to 0.4 (Figs. 6(d) and 7(d)) than 0.7.

The observational cases presented here represent almost the maximum possible difference in orientation of instrument axes relative to the anisotropic structures of LSC turbulence. LES predicts that these orientation differences should result in distinct differences in the slant beam estimates of vertical velocity variance, differences that agree with the observations qualitatively and to a large degree quantitatively. The field observations include sources of uncertainty that are not present in the numerical simulations. However the general agreement of the measured response functions, and of the differences between them, with those predicted by the LES encourages the conclusion that LES, sampled with the geometry of an ADCP, provides a powerful tool for the determination of response functions for turbulence quantities derived from ADCP slant beams.

7. Assessment of the predictive ability of theoretical response functions

Sensitivity of LES-derived response functions to interaction between horizontal beam orientation and large-eddy anisotropy, coupled with the non-universal quality of large-eddy characteristics, implies that deriving ADCP response functions by sampling LES

fields requires simulation of each particular type of turbulent flow. Since provision of such fields is a significant endeavor, we seek to assess the degree to which more easily calculated theoretical response functions have predictive ability, focusing first on the LSC case where both observations and LES are available and give reasonably similar results. We first note, however, that the "theoretical" responses calculated below must be considered only "quasi-theoretical," since they use observational estimates of anisotropy ratio and require at least some idea of phase relationships present (or absent) in the velocity field. Nonetheless if the theoretical response performs reasonably well in the case where both are known from the combination of observations and LES, we may have more confidence in using it to explore the range of response expected under differing assumptions about underlying turbulent structures.

The response function derived in Section 4 predicts that slant beam response in a turbulent flow depends on the dominant horizontal wavenumber of the large eddies, combined with anisotropy and phase effects, both of which may vary between different flows and, within a particular flow, with height above the instrument. Ideally we would determine the relevant parameters from observations and use them to predict response as a function of height. However observational determination of w_o/u_o presents a dilemma, since even if w' is available from a vertical beam, the available (first-order full-spread) estimates of horizontal velocity components,

$$u'_F = \frac{B_{2f} - B_{1f}}{2 \sin \theta} \tag{11}$$

$$v'_F = \frac{B_{4f} - B_{3f}}{2 \sin \theta} \tag{12}$$

are themselves affected by beam spread. We proceed by first assuming that the horizontal velocity components are <u>not</u> affected by beam spread and later consider likely effects of this assumption.

Vertical profiles of $\frac{w_o}{u_o} \equiv \frac{\sqrt{\langle u_3'^2 \rangle}}{\sqrt{\langle u_{1F}'^2 \rangle}}$ and $\frac{w_o}{v_o} \equiv \frac{\sqrt{\langle u_3'^2 \rangle}}{\sqrt{\langle u_{2F}^2 \rangle}}$ were determined for LSC using fluctuating horizontal velocities rotated into downwind (u'_{1F}) and crosswind (u'_{2F}) axes: $\langle w'^2 \rangle = \langle u_3'^2 \rangle$ is unaffected by this rotation. Variances are averages over the record length and error bars on the ratios are computed using estimated standard deviations (Appendix A) of the variances involved. Figure 10 shows resulting profiles for the LSC record (043.024) that has instrument beam planes most closely aligned downwind/crosswind. Within the rather large error bars, the two ratios agree and both have a significant increase with height, from values of order 0.2 near the bottom to values nearer 1 at $x_3/H \sim 0.7$, the maximum uncontaminated height accessible in the sea states that accompany LSC. Although measurements are unavailable for $x_3/H < 0.1$ due to finite size of the instrument package and possibly inaccurate above z_s, all ratios must approach zero as $w \rightarrow 0$ at $x_3/H = 0$ and 1. This approach to zero apparently occurs in relatively thin boundary layers at both surface and bottom of the water column.

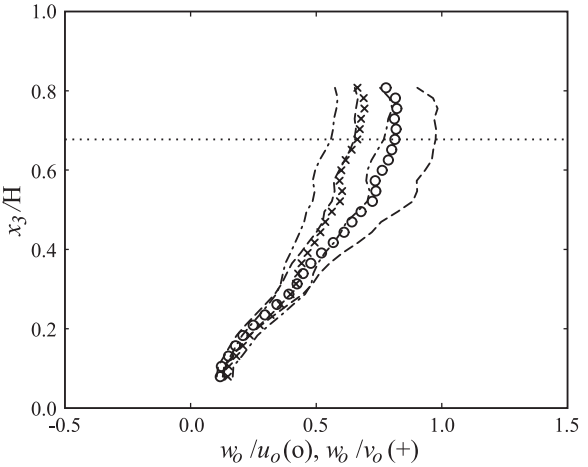

Figure 10. Profiles of $\frac{w_o}{u_o} \equiv \frac{\sqrt{\langle u_3'^2 \rangle}}{\sqrt{\langle u_{1F}'^2 \rangle}}$ (o) and $\frac{w_o}{v_o} \equiv \frac{\sqrt{\langle u_3'^2 \rangle}}{\sqrt{\langle u_{2F}'^2 \rangle}}$ (x) and their error bars (dash and dash-dot lines respectively), for LSC record 043.024. Horizontal velocities are downwind (o) and crosswind (x) components: $\langle u_3'^2 \rangle = \langle w'^2 \rangle$. The horizontal dashed line marks z_s.

Because there are even larger uncertainties involved in observational determination of ϕ_o, we instead specify simplified phase profiles consistent with the LSC characteristics cartooned in Figure 2. In the downwind plane, i.e. $u_3' = w' = -u_1'$ ($\phi_o = 180°$) throughout the water column. In the crosswind plane, u_3' lags u_2' by 90° ($\phi_o = -90°$) at the bottom and leads it by 90° ($\phi_o = +90°$) at the top: variation of phase with height is assumed to be linear, with zero-crossing at a height $x_3/H = 0.7$ suggested by the observations.

Figure 11 shows the LSC response function computed from Eq. (10) using observational values of w_o/u_o and w_o/v_o, the specified phase profiles, and values of $k_1 = 2\pi/160$ m and $k_2 = 2\pi/80$ m for downwind and crosswind wavenumbers, respectively. Because phase between u_3' and u_1' is constant with height, downwind response depends solely on w_o/u_o. Response is slightly greater than unity near the bottom, where $w_o/u_o \sim 0.2$ is below 0.577, the value associated with unity response, and decreases as w_o/u_o increases, becoming slightly less than unity in the upper half of the water column, where w_o/u_o exceeds 0.577. A downwind length scale of 160 m $\sim 18\Delta_M$ is sufficiently large that downwind response is near unity throughout the water column.

The crosswind response, involving height variation in both w_o/v_o and ϕ_o, predicts under-estimation below and over-estimation above $x_3/H \sim 0.7$, the height at which phase is assumed to shift from negative (below) to positive (above). This behavior, caused by dominance of response variation associated with phase over that associated with anisotropy ratio for observed values of the latter, agrees well with the LES crosswind response.

In summary, theoretical response calculations predict that for LSC large-eddy structures,

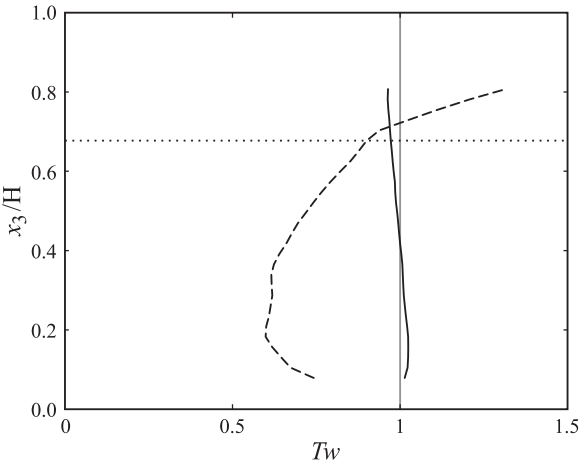

Figure 11. Theoretical vertical velocity response functions for downwind (solid line) and crosswind (dashed line) LSC components, computed from Eq. (10) using profiles of w_o/u_o (solid line: downwind) and w_o/v_o (dash line: crosswind) estimated from record 043.024 and an assumed form of phase variation with height above bottom. Assumed spatial scales are 160 m and 80 m for the downwind and crosswind components respectively. For details, see text.

turbulent vertical velocity variance calculated with a beam pair in the downwind plane will be quite accurate, while variance calculated with a pair in the crosswind plane will be an under-estimate of up to 40% in the lower part of the water column, switching to an over-estimate that rapidly approaches the same amount above $x_3/H \sim 0.7$. These predictions are qualitatively consistent with both observational and LES response functions. A quantitative difference is theoretical prediction of downwind response near unity, while LES and observational downwind responses are significantly lower. In the observations, such a difference could result from error in assumed instrument orientation relative to the wind (since misalignment corresponds to lower downwind response, cf Figs. 6 and 7), but this is not a possible source of error in the LES. We suggest that the difference instead arises from under-estimation (to be discussed below) of the value used for w_o/u_o in deriving the (quasi-)theoretical response: a larger value of w_o/u_o would produce a lower theoretical variance (Fig. 4(a)).

We now consider the convective case, for which we have only the observational response for comparison. Assuming first that the horizontal velocity component estimates are unaffected by beam spread, the example shown in Figure 12 has relatively uniform values of $w_o/u_o \sim w_o/v_o \sim 0.5$–$0.6$ over the observable water column. In the absence of phase effects, theory would predict nearly uniform, near-unity response with depth (Fig. 4(a)). Unfortunately, the phase structure of convective turbulence is not clearly defined by the observations, as it was in the LSC case. One might argue that the phase structure outlined above for the LSC crosswind velocity calculation is suitable for use in the convective case as well, since it describes generalized horizontal convergence (divergence) into a downwelling (upwelling) region at the surface and out of it (into it) at the

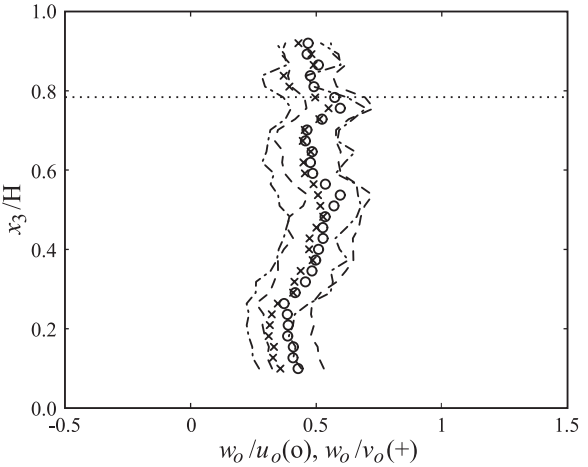

Figure 12. Profiles of $\frac{w_o}{u_o} \equiv \frac{\sqrt{\langle w'^2 \rangle}}{\sqrt{\langle u'^2 \rangle}}$ and $\frac{w_o}{v_o} \equiv \frac{\sqrt{\langle w'^2 \rangle}}{\sqrt{\langle v'^2 \rangle}}$ (x) and their error bars (dash and dash-dot lines respectively), for convection record 161.008. Convective velocity component variances are, within error bars, independent of coordinate system: here the components are in instrument coordinates.

bottom. One might further argue that such structure must be present in any arbitrary direction if convective features fill the water column and are roughly isotropic, as they appear to be. A variance response function can then be calculated with this phase structure, $k_1 = 2\pi/80$ m, and either of the orthogonal ratios. Because the imposed phase structure dominates vertical behavior of the response function when anisotropy ratios are roughly constant, the resulting vertical structure of the theoretical convective response functions (not shown) would closely resemble the LSC crosswind functions. The observed response (Fig. 3(c) and (d)) is instead nearly unity throughout the watercolumn, as predicted by the theoretical response in the absence of deterministic phase relationships. Modeling convective phase behavior instead as random variation of $\pm\Delta\phi_o \leq \pm 45°$ results in a response function with roughly the observed characteristics, suggesting that unstable convection is not characterized by the tight phase relationships present in LSC, at least within the part of the water column accessible to observation.

We finally return to the assumption of first-order homogeneity used in computing horizontal velocity variances. Clearly, if vertical velocity variance determined with this assumption is inaccurate, horizontal variances are likely to be inaccurate as well. LES results to be discussed in a subsequent paper indicate that for LSC, first-order expressions over-estimate both u_o and v_o throughout much of the water column. If the values used for u_o and v_o in the preceding calculations are over-estimates of the true values, the anisotropy ratios used are under-estimates and, from Figure 4(a), the calculated responses are over-estimates. Dominance of phase effects over those of the anisotropy ratio in the theoretical response function suggests that moderate over-

estimation of w_o/u_o should have relatively minor effect on predicted response for components characterized by strong depth-dependent phase relationships, ie the crosswind LSC response. However the downwind LSC response depends only on w_o/u_o, hence underestimation of w_o/u_o may be responsible for the over-estimated LSC downwind response remarked upon previously. We do not have comparable LES results for convectively driven turbulence. However the theoretical response function for turbulence without strong phase relationships will depend only on the anisotropy ratio, hence will be more significantly affected by inaccuracy in determination of horizontal velocity.

Although sampling an appropriate LES must be the preferred means of deriving response functions for turbulent quantities measured with an ADCP, the quasi-theoretical response function derived here appears to provide a useful tool for assessing potential effects of beam separation on measurements of turbulent vertical velocity variance.

8. Conclusions

We have used various methods to determine response functions for estimates of turbulent vertical velocity variance from slant beam measurements of a standard ADCP. An observational response function, using directly measured vertical velocity from a vertical acoustic beam, and a theoretical response function, derived for a beam pair estimate using salient turbulent large-eddy characteristics, have been determined for two quite different turbulent flows: full-depth Langmuir turbulence (LSC), characterized by horizontal anisotropy and strong phase relationships among velocity components, and unstable convection, characterized by horizontal isotropy and weak phase relationships. For LSC, an additional numerically-based response function has been derived by sampling stationary turbulent velocity fields of a LES with the geometry of an ADCP.

For LSC, all three response functions exhibit qualitatively consistent behavior, while the degree of quantitative agreement achieved seems reasonable, given uncertainties inherent in the measurements and the simplistic nature of the velocity field structure upon which the theoretical response is based. Both theoretical and LES methods demonstrate conclusively that the response is not inevitably an under-estimate that increases with range, as widely assumed. Instead, important characteristics of the turbulent large eddies, specifically quasi-deterministic phase relationships between horizontal and vertical velocities and vertical/horizontal anisotropy, can lead to over-estimation in parts of the range. The LES method demonstrates the additional importance of orientation of the instrument relative to horizontally anisotropic large-eddy structure, confirmed in differences between the two observational LSC cases presented here.

From the general agreement between theoretical and LES response functions, we conclude that the theoretical response function is a powerful tool for exploration of response sensitivity to parameters associated with the turbulent field and/or the instrument. As an aside, we note that this same theoretical response function can be applied to the

vertical velocity fields associated with internal waves, provided it is possible to determine their propagation direction (perhaps by tracking backscatter features across the 4-beam array, Scotti *et al.,* 2005), hence calculate their true horizontal length scale from apparent frequency. Necessary velocity component phase relationships can be supplied by linear/nonlinear internal wave theory.

The present observations, taken in two different types of turbulent flow with significant horizontal scales of $\sim$ 80 m in water of depth $\sim$ 15 m, suggest that given only slant beam velocities and lacking knowledge of velocity phase relations and/or instrument orientation relative to possible anisotropic structures, the "best" estimate of vertical velocity variance is not the 4-beam estimate normally used, but the larger of the two pair estimates. This "best" estimate is determined in a profile sense, by choosing the pair profile that is the larger over more than 50% of estimates below the level of sidelobe contamination. Applied to LSC turbulence, this algorithm would select the green profiles in both of the LES cases shown in Figure 6 and in the wind-aligned ($\psi = 0°$) observational case of Figure 9(a). In the $\psi = 45°$ cases, both pair estimates provide comparable values in the LES results of Figure 7, and selection is not crucial: in the observational case shown in Figure 9(b), the algorithm chooses the red profile. The algorithm also yields the profiles closest to true profiles for vertical velocity variances associated with convective turbulence and internal waves (not shown).

The LES results illustrate that in strongly anisotropic turbulence, differences among the various estimates can exceed those associated with the different slant beam angles ($\theta = 20°$ and $30°$) found in commercial Doppler profilers. Because the "best" estimate of vertical velocity variance is relatively insensitive to θ, (green curves in Fig. 8) and because (as will be shown in a subsequent paper) $\theta = 20°$ substantially degrades determination of horizontal velocity variances relative to $\theta = 30°$, we suggest that $\theta = 30°$ is preferable for measurement of turbulent quantities with an ADCP.

While the issue of eddy size relative to beam spread of ADCPs has long been realized (although, we would argue, not previously adequately addressed for turbulent flows), it has been sobering to realize the impacts on measurement of turbulent velocity variances of other non-universal characteristics of the energy-containing eddies. It should not, however, be automatically concluded that ADCPs cannot yield useful measurements of turbulence quantities. First, even an inaccurate estimate is better than none at all. Secondly, the success of the theoretical response function suggests that the quality and degree of inaccuracy can be at least roughly estimated using information about horizontal isotropy from forcing mechanisms (and the data itself) and estimates of vertical/horizontal anisotropy ratio from first-order fields. Finally there is the possibility, to be explored after examination of horizontal response functions in a subsequent paper, that variance measurements can be corrected iteratively, using observational estimates of anisotropy ratios and phases in the theoretical response.

Acknowledgments. We gratefully acknowledge the support for this research provided by grants from NOAA (NA06RU0139) and NSF (OCE-0136403).

APPENDIX A

Bias and spread of vertical velocity variance estimates

Estimates of vertical velocity variance made using squared beam velocities involve errors of both bias and spread. Bias error, associated with the presence of (assumed Gaussian random) noise in field measurements, is a positive offset from the "true" value that cannot be reduced by increased sample size, while spread refers to the statistical error associated with finite sample size. Spread reduction through increase in sample size is frequently not possible in geophysical measurements, where sampling can be limited by logistical constraints or, more frequently, by non-stationarity of the mean flow.

We first consider estimation of the variance of a product of fluctuation beam velocities, i.e. the variance $\langle B_{if}B_{jf}\rangle$, where angle brackets denote an average over N samples and $B_{if} \equiv B_i - \langle B_i\rangle$. We use the variance estimation method of Heathershaw and Simpson (1979, henceforth HS79), who derived a form for the ensemble variance σ^2_{uw} of the product of two possibly correlated signals u and w in terms of the observational N-sample variance $\langle\sigma^2_{uw}\rangle$ as

$$\sigma^2_{uw} \simeq \frac{\langle\sigma^2_{uw}\rangle}{MI}$$

where $MI = \dfrac{(1 + 2\Sigma)}{N}$ is the number of *independent* samples in N. Determination of MI involves summation $\Sigma = \sum_{i=2}^{L} \rho_{1,i}$ of the normalized covariance function $\rho_{1,i}$ through a maximum lag L beyond which covariance is negligibly small (taken here as the first zero-crossing: see HS79 for details). Note that since uncorrelated samples have $\rho_{1,i} \equiv 0$ for $i > 1$, hence $\Sigma = 0$, the variance estimate in this case reduces to the well known form $\sigma^2_{uw} \simeq \dfrac{\langle\sigma^2_{uw}\rangle}{N}$. Applying the method of HS79 to the product of fluctuating beam velocities, we use the notation $\sigma^2_{ij} \simeq \dfrac{\langle\sigma^2_{ij}\rangle}{MI}$, with associated ensemble standard deviation (std) $s_{ij} = (\sigma^2_{ij})^{1/2}$. MI, variances, and covariances are calculated separately for each beam and each bin. One std error bounds for the five variances and the six different covariances are shown for an LSC record in Figures A1 and A2 respectively. Since the variance calculation uses the observed signal, the resulting std includes random (spread) errors associated with both signal (the true velocity field) and noise.

We now consider bias in the observational case where beam velocity B_{if} contains both the actual beam velocity b_{if} plus noise n, i.e. $B_{if} = b_{if} \pm n$. For Gaussian noise that is uncorrelated with the velocity signal (as is the case for our deployment) Stacey *et al.* (1999) show that

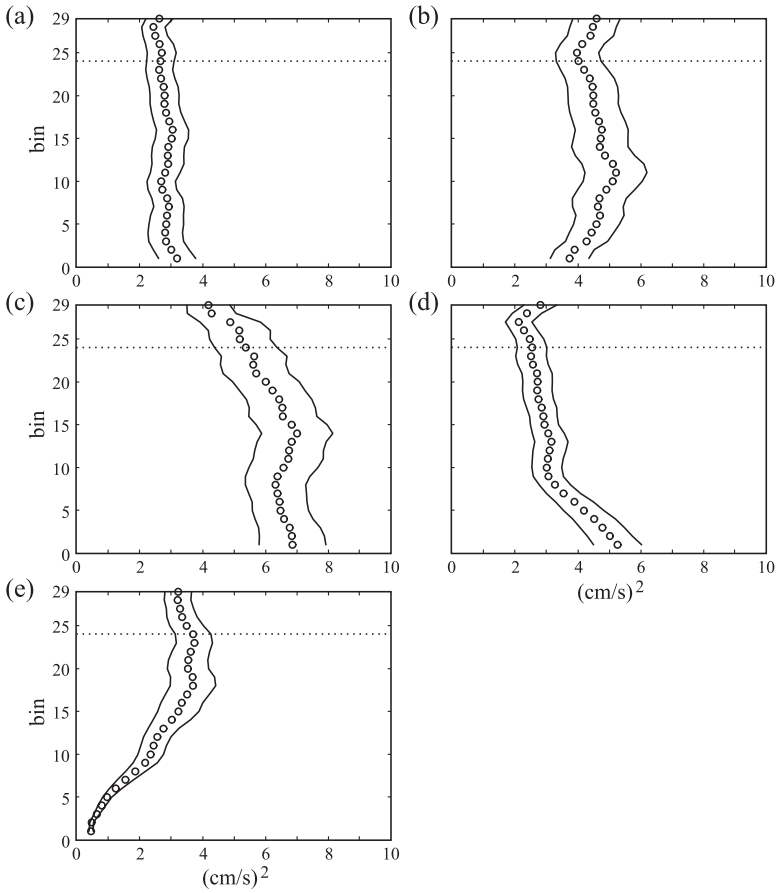

Figure A1. Beam velocity variances and associated one std error bars calculated by the method of HS79 for an LSC record (043.024), plotted as a function of range bin number (bin size = 0.4 m). (a)–(e), beams 1–5. Because of large surface wave displacements during this record, filtered vertical beam data are available only through bin 29, although the mean surface is in bin 36. Sidelobe contamination of slant beam data becomes possible above the dashed horizontal line: however as noted by GW07, acoustic backscatter from near-surface bubble clouds reduces the acoustical impact of the surface and sidelobe effects are rarely obvious in these conditions. Error bars can vary between beams and with range.

$$E(\langle B_{if}^2 \rangle) \equiv \frac{1}{N} \lim_{N \to \infty} \langle B_{if}^2 \rangle = \overline{b_i^2} + \sigma_n^2, \tag{A.1}$$

i.e. the expected value of the variance $E(\langle B_{if}^2 \rangle)$ is biased from the true (ensemble mean, denoted by an overbar) signal variance $\overline{b_i^2}$ by an amount equal to the noise variance σ_n^2. It remains to define the noise variance of the beam velocities.

Noise variance in a measurement situation depends on instrument noise level, subse-

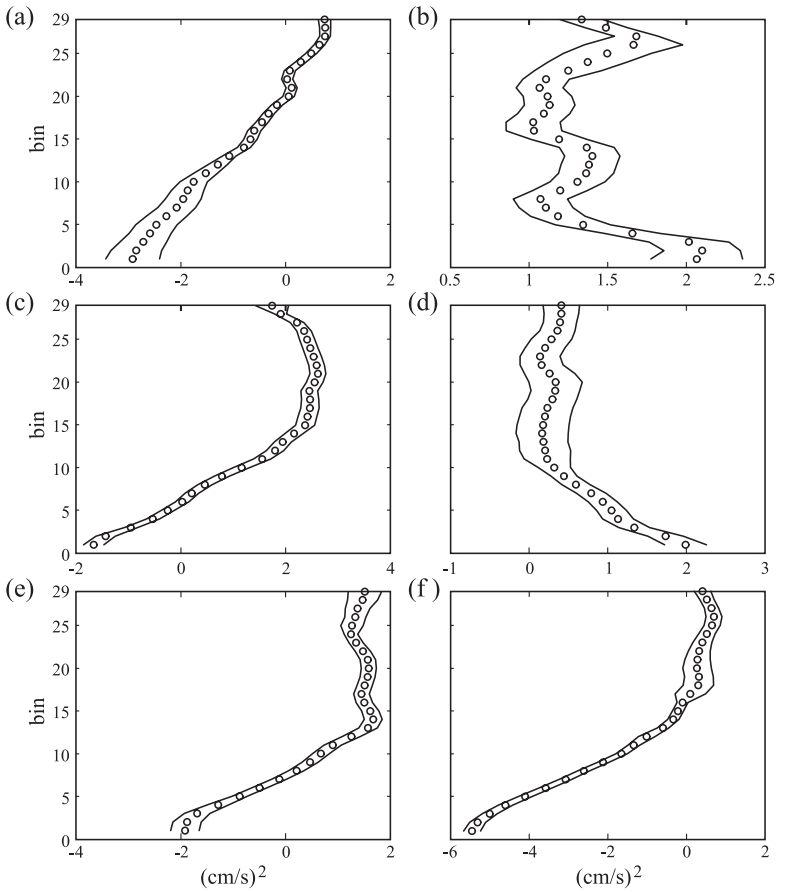

Figure A2. Beam velocity covariances $\langle B_{if} B_{jf} \rangle$ and one std error bars: $\{i, j\}$ = (a) {1,2} (b) {2,3} (c) {1,3} (d) {1,4} (e) {2,4} (f) {3,4}. Otherwise the same as Figure A1.

quent processing undertaken to reduce noise variance and, potentially, on specific deployment configuration. Because of the latter possibility, we attempt to determine the noise level of our processed data using *in situ* data. We choose noise records as those in which both vertical velocity and backscatter fields are essentially featureless, i.e. show no indication of a turbulent bottom boundary layer, internal waves, Langmuir circulations or unstable convection, all of which have distinctive velocity/backscatter signals. It is nonetheless difficult to achieve the true noise level of the slant beams. Even after the removal of a linear least-squares fit at each bin, used to reduce first order effects of non-stationarity in the data, the horizontal velocity field (which enters the slant beam velocities but not the vertical beam velocity) usually contains small residual changes on time scales comparable to the record length. While not noise in the instrumental sense, these variations nonetheless contribute residual variance to record-averaged slant beam

variance. This problem does not affect the vertical beam and vertical velocity variance is always the lowest measured during noise records. Over five noise records examined, the minimum vertical beam variance averaged over a record length was $\sigma_5^2 \cong 0.10 \pm 0.01(\text{cm/s})^2$. Because the physical location of the vertical beam is within the sidelobes of all four slant beams, it would be expected that the noise variance of the vertical beam would be, if anything, larger than that of a slant beam (because of their symmetrical arrangement relative to each other and to the vertical beam, all slant beams will be assumed to have equal noise variance σ_s^2). We thus interpret consistently larger slant beam variances in noise records as residual horizontal velocity variability present in the slant beams but absent from the vertical beam, and return later to the problem of determining σ_s^2. For now, proceeding with only the assumption of equal slant beam noise variances, it is easily shown that slant beam covariances $\langle B_{if}B_{jf}\rangle$, $i, j \neq 5$ are biased by the same amount as slant beam variances, i.e. high by σ_s^2.

Combining the effects of bias and spread yields

$$\overline{b_5 b_5} = E(\langle B_{5f}B_{5f}\rangle) - \sigma_5^2 = \langle B_{5f}B_{5f}\rangle - \sigma_5^2 \pm s_{55} \tag{A.2}$$

$$\overline{b_i b_j} = E(\langle B_{if}B_{jf}\rangle) - \sigma_s^2 = \langle B_{if}B_{jf}\rangle - \sigma_s^2 \pm s_{ij}, \quad i, j \neq 5. \tag{A.3}$$

With these expressions for the relationship of the desired ensemble-averaged beam (co)variances to the available record-averaged values, one can derive error bounds for the vertical velocity variance estimates considered in this paper.

The estimate $\langle w'^2\rangle = \langle B_{5f}^2\rangle$ made from the single vertical beam variance is related to true vertical velocity variance $\overline{w^2}$ by

$$\overline{w^2} = \langle w'^2\rangle - \sigma_5^2 \pm s_{55} \tag{A.4}$$

An estimate made from a pair of slant beams, e.g. Eq. (7)

$$\langle w_x'^2\rangle = \frac{\langle (B_{1f} + B_{2f})^2\rangle}{4\cos^2\theta} = \frac{\langle B_{1f}^2\rangle + 2\langle B_{1f}B_{2f}\rangle + \langle B_{2f}^2\rangle}{4\cos^2\theta}$$

involves beam covariances as well as variances. For equal slant beam noise variances, it is readily shown that

$$\begin{aligned}\overline{w^2} &= (4\cos^2\theta)^{-1}(\langle (B_{1f} + B_{2f})^2\rangle - 4\sigma_s^2 \pm (s_{11} + s_{22} + 2s_{12})) \\ &= \langle w_x'^2\rangle - \frac{\sigma_s^2}{\cos^2\theta} \pm \frac{(s_{11} + s_{22} + 2s_{12})}{4\cos^2\theta}\end{aligned} \tag{A.5}$$

where s_{12} is the std of the covariance of beams 1 and 2.

The standard 4-beam estimate of vertical velocity involves the square of the sum of all four slant beam velocities. It can be shown that

$$\overline{w^2} = \langle w_F'^2 \rangle - \frac{\sigma_s^2}{\cos^2\theta} \pm \frac{\left(\sum_{i=1}^{4} s_{ii} + \sum_{i=1}^{4} \sum_{j=1,\, j\neq i}^{4} s_{ij} \right)}{(4\cos\theta)^2}, \tag{A.6}$$

i.e. the 4-beam estimate has the same bias error as a pair estimate (as expected, since the 4-beam velocity is the average of the two 2-beam pair estimates) but spread influenced not only by the standard deviations of all four beam variances, but also by those of all possible different beam covariances. This does not necessarily mean that the spread of the 4-beam estimate is worse than that of pair estimates. If all covariances are identically zero and all beams have equal variance, then the spread of the 4-beam estimate is half that of a 2-beam estimate (a result of using twice the number of measurements). However, as documented previously (Figs. A1 and A2), neither of these conditions generally hold in a turbulent flow and spread errors in various estimates of $\overline{w^2}$ should be computed directly from observations.

We now return to the problem of determining $\sigma_s^2 \leq \sigma_5^2$, having previously concluded that excess slant beam variance relative to vertical beam variance in noise records resulted from residual horizontal velocity variability on scales comparable to record length. Effects of this residual variance will be minimized if the slant beams are used to calculate vertical velocity, since to first order this calculation removes large-scale horizontal velocity. In the noise record used to define σ_5^2,

$$\min\left(\langle w_F'^2 \rangle, \langle w_x'^2 \rangle, \langle w_y'^2 \rangle\right) = (\cos^2\theta)^{-1}\sigma_s^2 \simeq 0.03 \pm 0.04\ (\mathrm{cm/s})^2.$$

Although technically this value is not significantly different from zero, slant beam noise level is expected to be non-zero, and we will use the associated minimum value of $\sigma_s^2 \cong 0.02 \pm 0.03\ (\mathrm{cm/s})^2$ as the slant beam noise variance. As argued previously, one expects the slant beams to have a smaller noise level than the vertical beam. While a factor of 5 is uncomfortably large, results from comparison of various estimates of horizontal velocity variance, to be discussed in a subsequent paper, independently suggest that the vertical beam has a noise level substantially larger than that of the slant beams. We thus correct the vertical velocity variance estimates for noise bias using $\sigma_5^2 = 0.10(\mathrm{cm/s})^2$ and $\sigma_s^2 = 0.02\ (\mathrm{cm/s})^2$ in expressions (A.4)–(A.6). In records from a strongly turbulent flow, such as that associated with Langmuir supercells, bias corrections for the vertical velocity variance estimates are largely irrelevant, but become of more importance in records from weakly turbulent flows, such as those associated with unstable convection. An accurate method of determining *in situ* beam noise variances, separately for each beam, should be a goal of future work.

For representative records of (a) LSC and (b) convective turbulence, Figure A3 shows bias-corrected profiles of vertical velocity variances, comparing the vertical beam estimate with the two pair estimates and the 4-beam estimate. The one standard deviation error bars shown are calculated using observationally determined standard deviations of beam variances and covariances in the expressions of (A.4)–(A.6).

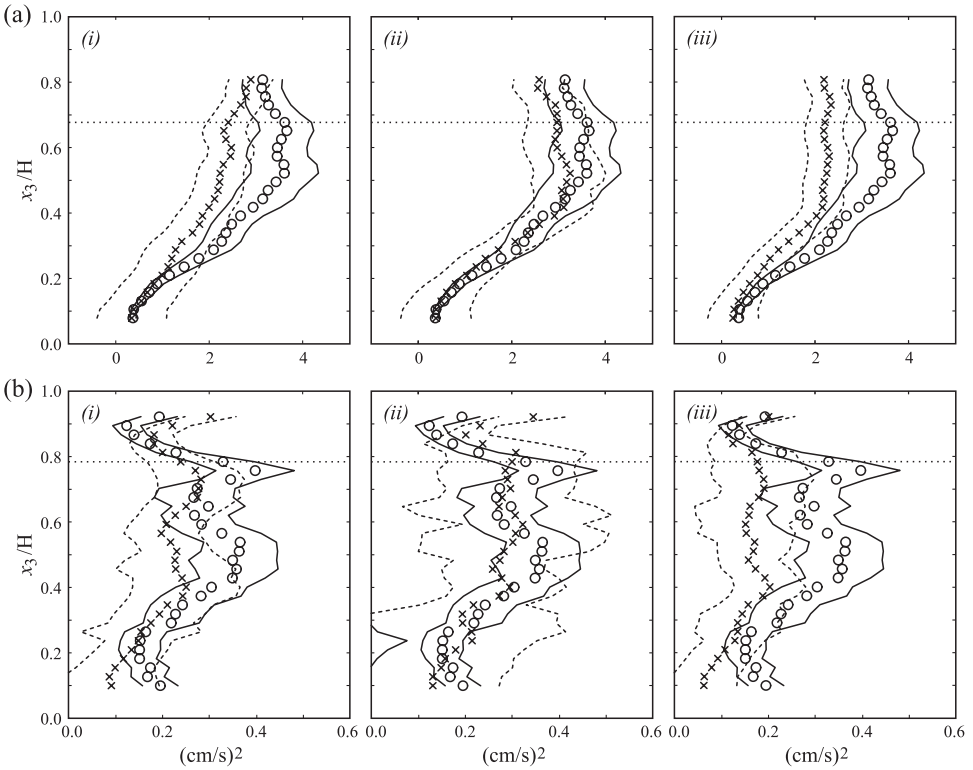

Figure A3. For a record of (a) LSC (043.024) and (b) unstable convection (161.008), panels compare the vertical beam estimate $\langle w'^2 \rangle$ (o) and its error bounds (solid lines) with slant beam estimates of vertical velocity variance (x) and their one standard deviation error bars (dashed lines): (*i*) $\langle w_x'^2 \rangle$, 2-beam estimate from the {2,1} pair (*ii*) $\langle w_y'^2 \rangle$, 2-beam estimate from the {4,3} pair (*iii*) $\langle w_F'^2 \rangle$, 4-beam estimate. All estimates are bias-corrected.

APPENDIX B

Determination of "ADCP" variances from LES

As described fully in TMG07, filtered Navier-Stokes equations with a subgrid-scale parameterization are solved to obtain resolved velocity (u_1, u_2, u_3) at each grid point in the domain. Using the classical Reynolds decomposition, the resolved velocity is $(u_1, u_2, u_3) = (\langle u_1 \rangle, \langle u_2 \rangle, \langle u_3 \rangle) + (u_1', u_2', u_3')$ in a Cartesian coordinate system (x_1, x_2, x_3) where x_1 is downwind direction, x_2 crosswind direction and x_3 the vertical direction: brackets denote averaging over time and over the two homogenous horizontal directions of the flow. The total beam velocity for beam q, B_q, is defined as the scalar projection of resolved velocity along the beam axis (positive in the direction toward the transducer),

$$B_q = -(n_1^q, n_2^q, n_3^q) \cdot (u_1, u_2, u_3) = -(n_1^q u_{q1} + n_2^q u_{q2} + n_3^q u_{q3})$$

where (n_1^q, n_2^q, n_3^q) is an outward unit vector along the axis of beam q and u_{qj} is the LES velocity at the $(x_{q1}(x_3), x_{q2}(x_3), x_3)$ location along the beam (dependence on x_3 will henceforth be omitted for simplicity in notation, but is implicit). The associated fluctuating beam velocity is $B_{qf} = B_q - \langle B_q \rangle$. If the instrument is aligned in the downwind direction ($\psi = 0$, defined as $\{x, y, z\} = \{x_1, x_2, x_3\}$), beam 1–5 unit vectors are

$$\begin{aligned}
(n_1^1, n_2^1, n_3^1) &= (\sin\theta, 0, \cos\theta)\\
(n_1^2, n_2^2, n_3^2) &= (-\sin\theta, 0, \cos\theta)\\
(n_1^3, n_2^3, n_3^3) &= (0, \sin\theta, \cos\theta)\\
(n_1^4, n_2^4, n_3^4) &= (0, -\sin\theta, \cos\theta)\\
(n_1^5, n_2^5, n_3^5) &= (0, 0, 1)
\end{aligned}$$

For ease of notation in what follows, we now let $(u_1, u_2, u_3) = (u, v, w)$, thus $u_{q1} = u_q$, $u_{q2} = v_q$, and $u_{q3} = w_q$. Then, for example, beam 1 velocity and its fluctuating counterpart can be written as

$$\begin{aligned}
B_1 &= -(\sin\theta, 0, \cos\theta)\cdot(u_1, v_1, w_1) = (-u_1 \sin\theta - w_1 \cos\theta)\\
B_{1f} &= -(\sin\theta, 0, \cos\theta)\cdot(u_1', v_1', w_1') = (-u_1' \sin\theta - w_1' \cos\theta).
\end{aligned} \tag{B.1}$$

The beam 5 variance calculation is straightforward. To illustrate computation of variances based on the slant beams, consider the expression for vertical velocity variance based on the vertical velocity calculated from beams 1 and 2 (i.e. Eq. (7)):

$$\langle w_x'^2 \rangle = \frac{\langle (B_{1f} + B_{2f})^2 \rangle}{4\cos^2\theta} \tag{B.2}$$

Inserting expression (B.1) and a similar expression for beam 2 into (B.2) leads to

$$\langle w_x'^2 \rangle = \frac{A + B}{4\cos^2\theta} \tag{B.3}$$

where

$$A = \sin^2\theta\langle u_1'u_1'\rangle + \sin^2\theta\langle u_2'u_2'\rangle + \cos^2\theta\langle w_1'w_1'\rangle + \cos^2\theta\langle w_2'w_2'\rangle$$

$$B = -2\sin^2\theta\langle u_1'u_2'\rangle + 2\cos^2\theta\langle w_1'w_2'\rangle + 2\sin\theta\cos\theta\langle u_1'w_2'\rangle - 2\sin\theta\cos\theta\langle u_2'w_1'\rangle.$$

As a result of the averaging employed, $\langle u_1'u_1'\rangle = \langle u_2'u_2'\rangle = \langle u'u'\rangle$ and $\langle w_1'w_1'\rangle = \langle w_2'w_2'\rangle = \langle w'w'\rangle$, where $\langle u'u'\rangle$ and $\langle w'w'\rangle$ are streamwise and vertical variances, available from the LES at every vertical grid level. The necessary two-point auto- and cross-correlations, $\langle u_1'u_2'\rangle = \langle u'(x + \Delta)u'(x - \Delta)\rangle$, $\langle w_1'w_2'\rangle = \langle w'(x + \Delta)w'(x - \Delta)\rangle$, $\langle u_1'w_2'\rangle = \langle u'(x + \Delta)w'(x - \Delta)\rangle$ and $\langle u_2'w_1'\rangle = \langle u'(x - \Delta)w'(x + \Delta)\rangle$ where $\Delta = z\tan\theta$, are evaluated at

each vertical grid level[14], enabling calculation of $\langle w_x'^2 \rangle$ through Eq. (B.3). Note that Eq. (B.3) reduces to an identity when θ and thus Δ are zero, as expected. Estimates for vertical variances based on equations (6) and (8) are obtained in a similar fashion.

Expressions for the "sampled" variances in terms of one-point and two-point correlations are (relatively) simple for the case when the instrument is aligned in the downwind direction, i.e. $\psi = 0$. When $\psi \neq 0$, the resulting expressions, given in terms of two-dimensional two-point correlations, are quite extensive and not practical for presentation. However they can be rapidly and accurately obtained via symbolic algebra packages such as Maple or Mathematica.

14. The LES provides two-point correlations at distances $n\delta x$ where δx is the computational grid spacing in x and $n = \ldots, -3, -2.1, 0, 1, 2, 3, \ldots$. Since beam locations in the horizontal do not necessarily correspond to one of the computational grid points, we use linear interpolation to provide the two-point correlations at the required beam location.

REFERENCES

Cheng, R. T., C.-H. Ling, J. W. Gartner and P. F. Wang. 1999. Estimates of bottom roughness length and bottom shear stress in South San Francisco Bay, California. J. Geophys. Res., *104,* 7715–7728.

Christopher, R. S., J. R. Lacy and G. Voulgaris. 2006. Shear velocity estimates on the inner shelf off Grays Harbor, Washington, USA. Cont. Shelf Res., *26,* 1995–2018, doi:10.1016/j.csr.2006.07.025.

Gargett, A. E. 1994. Observing turbulence with a modified acoustic Doppler current profiler. J. Atmosph. Oceanic Tech., *11,* 1592–1610.

Gargett, A. E., T. R. Osborn and P. W. Nasmyth. 1984. Local isotropy and the decay of turbulence in a stratified fluid. J. Fluid Mech., *144,* 231–280.

Gargett, A. E. and J. R. Wells. 2007. Langmuir turbulence in shallow water: Part I. Observations. J. Fluid Mech., *576,* 27–61.

Gargett, A. E., J. R. Wells, A. E. Tejada-Martínez and C. E. Grosch. 2004. Langmuir supercells: a mechanism for sediment resuspension and transport in shallow seas. Science, *306,* 1925–1928.

Goodman, L. 1990. Acoustic scattering from ocean microstructure. J. Geophys. Res., *95,* 11,557–11,573.

Heathershaw, A. D. and J. H. Simpson. 1978. The sampling variability of the Reynolds stress and its relation to boundary shear stress and drag coefficient measurements. Est. Coastal Mar. Sci., *6,* 263–274.

Lu, Y. and R. G. Lueck. 1999. Using a broad-band ADCP in a tidal channel. Part II. Turbulence. J. Atmosph. Oceanic Tech., *16,* 1568–1579.

McWilliams, J. C., P. P. Sullivan and C.-H. Moeng. 1997. Langmuir turbulence in the ocean. J. Fluid Mech., *334,* 1–30.

Osborn, T. R. and R. G. Lueck. 1985. Turbulence measurements from a submarine. J. Phys. Oceanogr., *15,* 1502–1520.

Rippeth, T. P., E. Williams and J. H. Simpson. 2002. Reynolds stress and turbulent energy production in a tidal channel. J. Phys. Oceanogr., *32,* 1242–1251.

Scotti, A., B. Butman, R. C. Beardsley, P. S. Alexander and S. Anderson. 2005. A modified beam-to-earth transformation to measure short-wavelength internal waves with an Acoustic Doppler Current Profiler (ADCP). J. Atmosph. Oceanic Tech., *22,* 583–591.

Stacey, M. T., S. G. Monismith and J. R. Burau. 1999. Measurements of Reynolds stress profiles in unstratified tidal flow. J. Geophys. Res., *104,* 10,933–10,949.

Stanton, T. P. 2001. A Turbulence-Resolving Coherent Acoustic Sediment Flux Probe and Method for Using. US Patent 6,262,942, issued 17 July 2001.

Tejada-Martínez, A. E. and C. E. Grosch. 2007. Langmuir turbulence in shallow water: Part II. Large-eddy simulation. J. Fluid Mech., *576,* 63–108.

Theriault, K. B. 1986. Incoherent multibeam Doppler current profiler performance Part II – Spatial response. IEEE J. Oceanic Eng., *OE-11,* 16–25.

Thorpe, S. A. and J. M. Brubaker. 1983. Observations of sound reflection by temperature microstructure. Limnol. Oceanogr., *28,* 601–613.

Thorpe, S. A., T. R. Osborn, J. Jackson, A. J. Hall and R. G. Lueck. 2003. Measurements of turbulence in the upper ocean using Autosub. J. Phys. Oceanogr., *33,* 122–145.

Wells, J. R. and A. E. Gargett. 2008. Langmuir circulation on the continental shelf: A comparison of forcing conditions. (in prep.)

Received: *29 November, 2007;* revised: *14 April, 2008.*